Improvement of light extraction in organic light-emitting diodes using a corrugated microcavity

Bo Jiao,[1] Yue Yu,[1] Yang Dai,[1] Xun Hou,[1] and Zhaoxin Wu[1*]

[1] *Key Laboratory for Physical Electronics and Devices of the Ministry of Education & Shaanxi Key Lab of Information Photonic Technique, School of Electronicand Information Engineering, Xi'an Jiaotong University, Xi'an, 710049, China*

** zhaoxinwu@ mail.xjtu.edu.cn*

Abstract: Based on the phase separation effect in the film formation process of Polystyrene and Poly(methyl methacrylate) blend solution, bottom-emitting organic light-emitting diodes (OLEDs) with corrugated microcavity was demonstrated. This device exhibited high efficiency, broad spectra and Lambertian angular emission. Compared with the traditional bottom-emitting OLEDs with ITO anode and the planar microcavity OLEDs, about 57% and 41% enhancement for external quantum efficiency was achieved in this corrugated microcavity OLEDs respectively. This improvement can be understood by the scattering effect of the quasi-periodic characteristic of this corrugated microcavity which reduces the optical loss at surface plasmon polariton modes and wave-guided modes. This work provides a simple as well as efficient method to recover trapped light in OLEDs, which will benefit the low cost fabrication process.

OCIS codes: (230.0230) Optical devices; (230.3670) Light-emitting diodes; (230.4000) Microstructure fabrication.

References and links

1. L. S. Hung and C. H. Chen, "Recent progress of molecular organic electroluminescent materials and devices," Mater. Sci. Eng. R-Rep. **39**(5-6), 143–222 (2002).
2. S. Reineke, F. Lindner, G. Schwartz, N. Seidler, K. Walzer, B. Lüssem, and K. Leo, "White organic light-emitting diodes with fluorescent tube efficiency," Nature **459**(7244), 234–238 (2009).
3. T. Urabe, "The outstanding potential of OLED displays for TV applications," Information Display **24**, 14–17 (2008).
4. K. Saxena, V. K. Jain, and D. S. Mehta, "A review on the light extraction techniques in organic electroluminescent devices," Opt. Mater. **32**(1), 221–233 (2009).
5. R. Meerheim, M. Furno, S. Hofmann, B. Lüssem, and K. Leo, "Quantification of energy loss mechanisms in organic light-emitting diodes," Appl. Phys. Lett. **97**(25), 253305 (2010).
6. Y.-G. Bi, J. Feng, Y.-F. Li, Y. Jin, Y.-F. Liu, Q.-D. Chen, and H.-B. Sun, "Enhanced efficiency of organic light-emitting devices with metallic electrodes by integrating periodically corrugated structure," Appl. Phys. Lett. **100**(5), 053304 (2012).
7. T. Schwab, C. Fuchs, R. Scholz, A. Zakhidov, K. Leo, and M. C. Gather, "Coherent mode coupling in highly efficient top-emitting OLEDs on periodically corrugated substrates," Opt. Express **22**(7), 7524–7537 (2014).
8. Y. H. Kim, J. Lee, W. M. Kim, C. Fuchs, S. Hofmann, H.-W. Chang, M. C. Gather, L. Mueller-Meskamp, and K. Leo, "We Want Our Photons Back: Simple Nanostructures for White Organic Light-Emitting Diode Outcoupling," Adv. Funct. Mater. **24**(17), 2553–2559 (2014).
9. W. H. Koo, S. M. Jeong, F. Araoka, K. Ishikawa, S. Nishimura, T. Toyooka, and H. Takezoe, "Light extraction from organic light-emitting diodes enhanced by spontaneously formed buckles," Nat. Photonics **4**(4), 222–226 (2010).
10. S. Moller and S. R. Forrest, "Improved light out-coupling in organic light emitting diodes employing ordered microlens arrays," J. Appl. Phys. **91**(5), 3324–3327 (2002).
11. H.-Y. Lin, Y.-H. Ho, J.-H. Lee, K.-Y. Chen, J.-H. Fang, S.-C. Hsu, M.-K. Wei, H.-Y. Lin, J.-H. Tsai, and T.-C. Wu, "Patterned microlens array for efficiency improvement of small-pixelated organic light-emitting devices," Opt. Express **16**(15), 11044–11051 (2008).

#225930 - $15.00 USD Received 31 Oct 2014; revised 11 Jan 2015; accepted 15 Jan 2015; published 10 Feb 2015

12. Y. Sun and S. R. Forrest, "Enhanced light out-coupling of organic light-emitting devices using embedded low-index grids," Nat. Photonics **2**(8), 483–487 (2008).
13. K. Ishihara, M. Fujita, I. Matsubara, T. Asano, S. Noda, H. Ohata, A. Hirasawa, H. Nakada, and N. Shimoji, "Organic light-emitting diodes with photonic crystals on glass substrate fabricated by nanoimprint lithography," Appl. Phys. Lett. **90**(11), 111114 (2007).
14. J.-W. Shin, D.-H. Cho, J. Moon, C. W. Joo, S. K. Park, J. Lee, J.-H. Han, N. S. Cho, J. Hwang, J. W. Huh, H. Y. Chu, and J.-I. Lee, "Random nano-structures as light extraction functionals for organic light-emitting diode applications," Org. Electron. **15**(1), 196–202 (2014).
15. S. J. Park, Y. D. Kim, H. W. Lee, H. J. Yang, J. Y. Cho, Y. K. Kim, and H. Lee, "Enhancement of light extraction efficiency of OLEDs using Si_3N_4-based optical scattering layer," Opt. Express **22**(10), 12392–12397 (2014).
16. X. Zhao, Z. Wu, S. Ning, S. Liang, D. Wang, and X. Hou, "Random lasing from granular surface of waveguide with blends of PS and PMMA," Opt. Express **19**(17), 16126–16131 (2011).
17. S. Walheim, M. Boltau, J. Mlynek, G. Krausch, and U. Steiner, "Structure formation via polymer demixing in spin-cast films," Macromolecules **30**(17), 4995–5003 (1997).
18. B. Jiao, Z. X. Wu, X. W. Yan, and X. Hou, "Influence of the thickness of N,N'-Bis(naphthalene-1-yl)-N,N'-bis(phenyl) benzidine layer on the performance of organic light-emitting diodes," Appl. Phys., A Mater. Sci. Process. **98**(1), 239–243 (2010).
19. Z. B. Wang, M. G. Helander, J. Qiu, D. P. Puzzo, M. T. Greiner, Z. M. Hudson, S. Wang, Z. W. Liu, and Z. H. Lu, "Unlocking the full potential of organic light-emitting diodes on flexible plastic," Nat. Photonics **5**(12), 753–757 (2011).
20. X. L. Zhu, J. X. Sun, X. M. Yu, M. Wong, and H. S. Kwok, "Investigation of Al- and Ag-based top-emitting organic light-emitting diodes with metal oxides as hole-injection layer," Japanese Journal of Applied Physics Part 1-Regular Papers Brief Communications & Review Papers **46**(3A), 1033–1036 (2007).
21. L. H. Smith, J. A. E. Wasey, I. D. W. Samuel, and W. L. Barnes, "Light Out-Coupling Efficiencies of Organic Light-Emitting Diode Structures and the Effect of Photoluminescence Quantum Yield," Adv. Funct. Mater. **15**(11), 1839–1844 (2005).
22. S. Wedge and W. L. Barnes, "Surface plasmon-polariton mediated light emission through thin metal films," Opt. Express **12**(16), 3673–3685 (2004).
23. W. L. Barnes, A. Dereux, and T. W. Ebbesen, "Surface plasmon subwavelength optics," Nature **424**(6950), 824–830 (2003).
24. M. Fujita, K. Ishihara, T. Ueno, T. Asano, S. Noda, H. Ohata, T. Tsuji, H. Nakada, and N. Shimoji, "Optical and electrical characteristics of organic light-emitting diodes with two-dimensional photonic crystals in organic/electrode layers," Jpn. J. Appl. Phys. Part 1 -Regular Papers Brief Communications & Review Papers. **44**(Part 1), 3669–3677 (2005).

1. Introduction

Organic light emitting diodes (OLEDs) have attracted enormous attention due to their unique electrical and optical properties, including low-operating voltage, quick response time, self-emissive feature, emotion-friendly spectrum, and flexibility [1–3]. However, low light extraction efficiency still hamper the enhancement of OLEDs efficiency. A large part of generated light is trapped within the device as surface plasmon polariton (SPP) modes in the organic/metal interface and as waveguide modes in the glass substrate and the ITO/organic layers [4, 5]. To recover the trapped light, several approaches have been demonstrated, such as the use of periodical corrugated structures [6, 7], metal oxide embedded nanostructures [8], or quasi-periodic buckling structures [9] to extract SPP and waveguide modes, and the use of microlenses [10, 11], low index grids [12], photonic crystals [13], or nanostructure scattering layer [14, 15] to extract waveguide modes in OLEDs. Although some problems that once disturb the application of light extraction technology, such as wavelength dependency and viewing angle dependency, have been partially solved in recent progress, the complicated and expensive fabrication process of these approaches is still not suitable for the real application. In this work, we presented a simple corrugated microcavity structure to recover the trapped light. This corrugated microcavity OLEDs are fabricated on a polymeric nano-structure substrate, which is produced spontaneously by the phase separation effect in spin-coating of Polystyrene (PS) and Poly(methyl methacrylate) (PMMA) blend solution [16]. Compared with the control device, this corrugated microcavity OLEDs exhibits high efficiency, broad spectra and Lambertian angular emission. Furthermore, because of the quasi random structure of the corrugated microcavity, problems such as wavelength dependency and viewing angle dependency, that once disturbed the application of traditional planar microcavity OLEDs, can be solved effectively.

#225930 - $15.00 USD Received 31 Oct 2014; revised 11 Jan 2015; accepted 15 Jan 2015; published 10 Feb 2015

2. Experimental details

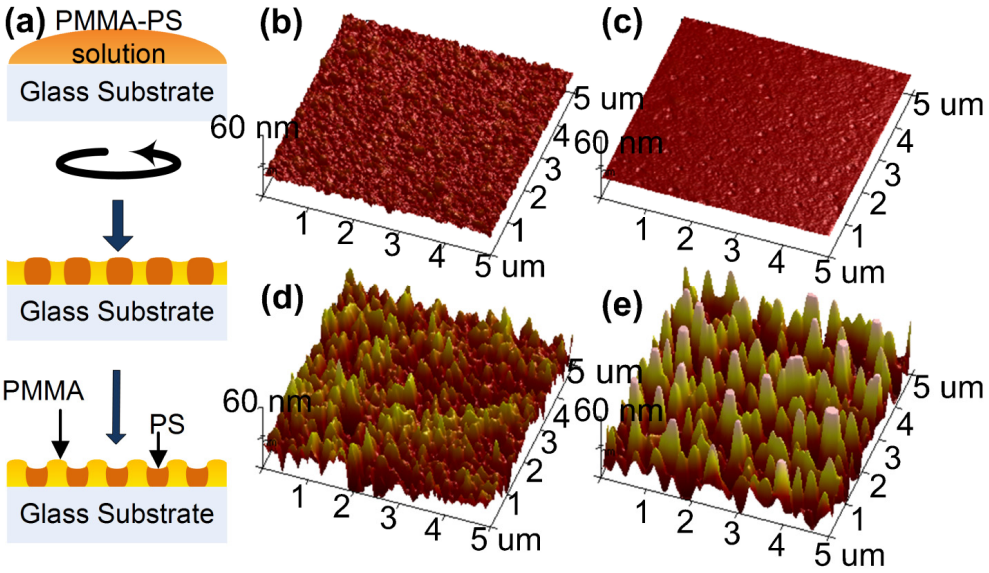

Fig. 1. (a) The schematic illustration for the fabrication of the PMMA-PS nano-structure. (b)-(e) AFM image of surface morphologies of ITO film (b), PMMA film (c), PS film (d), and PMMA-PS film (e) respectively.

The preparation process of the PS-PMMA film is shown in Fig. 1(a). PS (MW = 250 K) and PMMA (MW = 350 K), purchased from ACROS and Alfa Aesar, are dissolved in tetrahydrofuran (THF) with concentrations of 20 mg/ml, respectively. Then the solutions of these two polymers are mixed in the desired proportions. The ratio of PMMA and PS is optimized to be 8:2 wt and the blends solution concentration was 10 mg/ml. Before fabricating the nano-structure, the glass substrate is cleaned with deionized water, acetone and ethanol. Then the PMMA-PS blend solution is dropped on the pre-clean glass substrate. The origin of the phase separation of PMMA-PS lies in the different solubility of PMMA and PS in the THF [16, 17]. PMMA has a higher solubility in THF than PS. Therefore, during the spin-coating process, PS is more quickly depleted of the solvent and solidifies first onto the substrate during the volatilization process of THF, while PMMA tends to stay longer in the solvent. This leads the PMMA is elevated to form the island-like phase. Finally the film is annealed in oven at 70 °C for 30 minutes. The PS and the PMMA films are also fabricated by spin-coating process respectively as control group. The surface morphologies of the ITO, PMMA, PS and PMMA-PS are measured by atomic force microscope (AFM) system (NT-MDT Solver Pro). The surface of ITO and PMMA is flat (Fig. 1(b) and 1(c)). The PS film shows an amorphous rough surface (Fig. 1(d)) while the PMMA-PS film shows two-dimensional island-like nanostructures with the depths of 50-70 nm. The root-mean-square (RMS) roughness values of the ITO, PMMA, PS and PMMA-PS film are 2.4 nm, 0.459 nm, 15.7 nm and 23.4 nm respectively.

The light emitting section of the OLEDs were all fabricated by vacuum thermal evaporation process. For control device using ITO as anode, 100-nm-thick ITO-coated glass with a sheet resistance of 25Ω/□ was used as substrate. Prior to organic layer deposition, ITO substrate was cleaned with deionized water and organic solvents, and then exposed to an UV-ozone ambient for 1 min. For device using Ag anode, the UV-ozone treatment was cancelled to protect the corrugated structure under the Ag anode film. An ultrathin MoO_3 layer with the thickness of 1 nm was used to improve the hole injection of the Ag anode. All organic materials were deposited at the base pressure of 1×10^{-3} Pa with the evaporation rate around 0.2 nm/s. LiF and

#225930 - $15.00 USD Received 31 Oct 2014; revised 11 Jan 2015; accepted 15 Jan 2015; published 10 Feb 2015

Al were deposited without breaking the vacuum. The evaporation rates of MoO_3 and LiF are around 0.1 nm/s. And the evaporation rates of Ag film and Al film are 1nm/s and 5nm/s respectively. The thickness of the films was determined in situ by a quartz-crystal sensor and *ex situ* by a profilometer. Active area of devices was 12 mm^2 for all the samples studied in this work. The current-voltage-luminance characteristics of the devices were measured by a computer-controlled doucement (Keithley 2602). All the measurements were carried out at room temperature under ambient conditions. The PR650 spectrophotometer and Fiber Optic Spectrometer is utilized to measure the electroluminescent spectra. The corrugated OLEDs was also characterized by scanning electronic microscopy (SEM, FEI Quanta 250 FEG Serials).

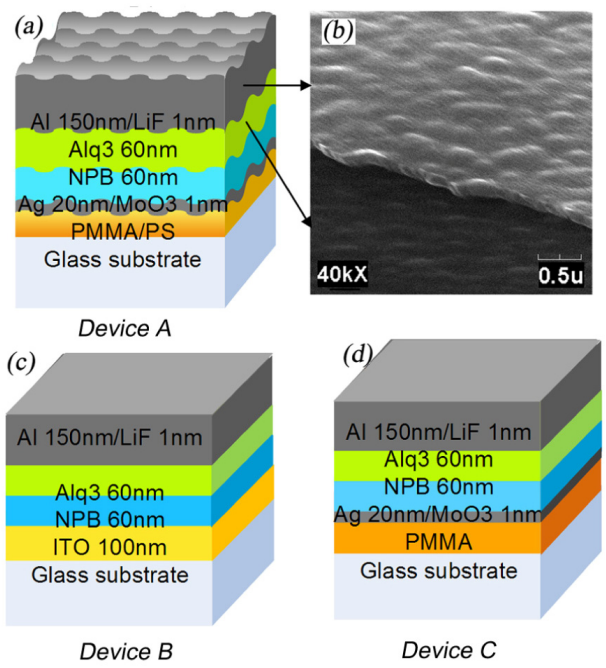

Fig. 2. (a) Schematic structure of the OLEDs based on PMMA-PS nano-structure (device A). (b) Scanning electron microscope image of the organic and aluminum layer viewing from the top of this OLEDs. Schematic structures of the two control devices, device B (c) and device C (d),respectively.

To examine the influence of PMMA-PS nano-structure substrate on the device performance, a bottom-emitting OLEDs with structure of Glass/ PMMA-PS nano-structure/ Ag (20 nm)/ MoO_3 (1 nm)/ N-N′-diphenyl-N-N′-bis(1-naphthyl)-1,1’-biphenyl-4,4′-diamine (NPB) (60 nm)/ tris(8-hydroxyquinoline) aluminium (Alq_3) (60 nm)/LiF (1 nm)/ Al(150nm) (Device A) was fabricated, just as shown in Fig. 2(a). Here, thin Ag film and the Al film were used as anode and cathode respectively. The thickness of Ag film is crucial for the device performance. On the one hand, the silver layer acts as anode for the OLEDs. Thus, enough thickness is needed to conduct electrical current. On the other hand, strong reflection effect of thick silver film will decrease the light outcoupling from the Ag anode side, which will harm the device performance seriously. The optimal silver thickness in our study is around 20 nm. NPB was used as hole transport layer, and Alq_3 was used as green emission layer as well as electron transport layer. MoO_3 layer and LiF layer were used as hole-injection layer and electron-injection layer respectively. The SEM image of the organic and aluminum layer viewing from the top of this OLEDs, as shown in Fig. 2(b), demonstrates that the corrugated morphology of PMMA-PS layer has been well preserved on each layer, which confirms the corrugation structure of all layers. Traditionally, ITO substrate is used as anode in

#225930 - $15.00 USD Received 31 Oct 2014; revised 11 Jan 2015; accepted 15 Jan 2015; published 10 Feb 2015

bottom-emitting OLEDs [18]. Thus, a OLEDs with structure of ITO/ NPB (60 nm)/ Alq_3 (60 nm)/LiF (1 nm)/ Al(150nm) (Device B) was fabricated as control device, just as shown in Fig. 2(c). Besides, a strong optical microcavity will be formed in device A because both the anode and the cathode of device A are metal. So, the photo density of stated will be redistributed and the spontaneous emission intensity of certain wavelengths can be enhanced in a given direction in the microcavity structure. It has been demonstrated that this microcavity effect is a important approach for achieving high efficiency OLEDs [19]. Thus, to study the different influence between the traditional planar microcavity and our corrugated microcavity on the performance of OLEDs, a planar microcavity OLEDs using Ag as anode and Al as cathode was also fabricated as control device. The structure of the planar microcavity OLEDs is Glass/ Ag (20 nm)/ MoO_3 (1 nm)/ NPB (60 nm)/ Alq_3 (60 nm)/LiF (1 nm)/ Al(150nm) (Device C).

3. Results and discussion

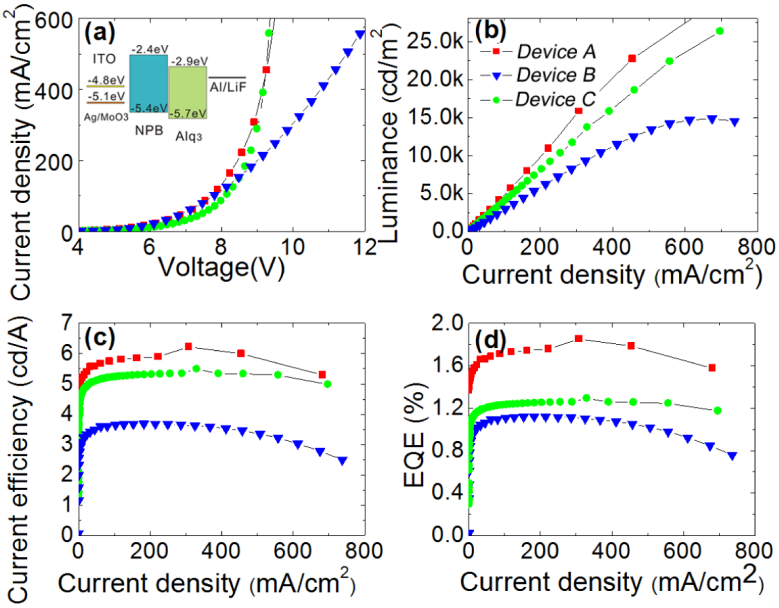

Fig. 3. Current density-voltage characteristics (a), luminance-current density characteristics (b), current efficiency-current density characteristics (c), and external quantum efficiency (EQE) -current density characteristics(d) of devices A, B, and C, respectively. The insert in (a) is the energy diagram of ITO-based OLEDs and Ag-based OLEDs

As demonstrated by Koo et. al [9] and Zhu et. al [20], MoO_3 is an excellent modification layer for Ag anode. The effective work function of Ag/MoO_3 anode is about −5.1eV [20], which is larger than that of ITO anode (~-4.8eV). Thus, the hole injection barrier between Ag/MoO_3 anode and NPB hole transporting layer is smaller than that between ITO and NPB, as shown in insert of Fig. 3(a). Because of the better hole-injection property of Ag/MoO_3 anode, just as shown in Fig. 3(a) and 3(b), both of the planar and corrugated microcavity OLEDs (devices A and C) exhibit lower driven voltage as well as higher luminance than the ITO-based OLEDs (device B) at the same current density. The current efficiency-current density characteristics of devices A, B and C are shown in Fig. 3(c). At the same current density of 160 mA/cm^2, the current efficiency of device A with corrugated structure is 6.0 cd/A, while that of the device B based on ITO anode and device C based on planar microcavity are 3.6 cd/A and 5.3cd/A respectively. Compared with the control device B and C, the current efficiency of device A is enhanced by 67% and 11% respectively. The external quantum efficiency (EQE) of these devices are shown in Fig. 3(d). The EQE of device A with PMMA-PS nano-structure reaches

#225930 - $15.00 USD Received 31 Oct 2014; revised 11 Jan 2015; accepted 15 Jan 2015; published 10 Feb 2015

1.76%, which is 1.57 times and 1.41 times as high as that of the device B with ITO anode and the device C with planar microcavity respectively.

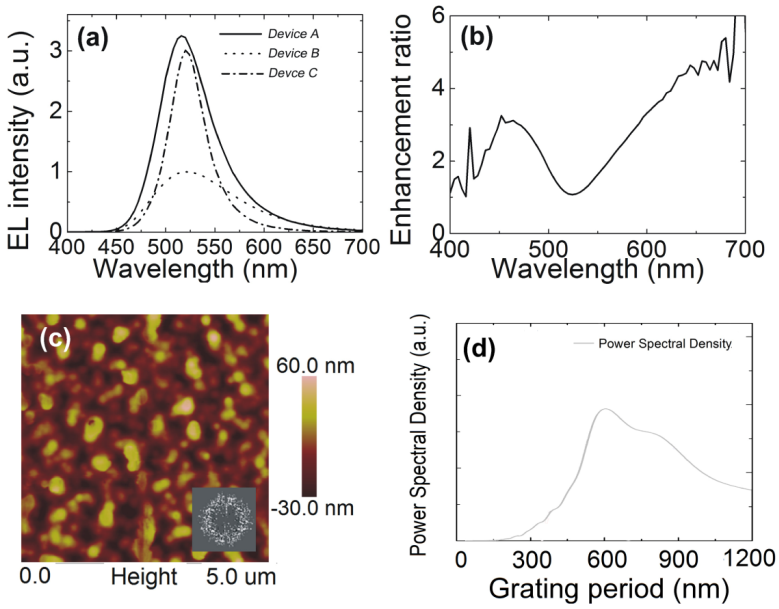

Fig. 4. (a) The normalized electroluminescence spectra of device A (solid line), device B (dot line), and device C (dot and dash line) from normal direction respectively. (b) Enhancement ratio of intensity by corrugated structure as a function of wavelength. (c) 2D AFM image of PMMA-PS film, inset image is the FFT pattern. (d) The power spectrum from FTT as a function of grating period.

Figure 4(a) shows the EL spectra of the device A with corrugated microcavity, device B using ITO anode, and device C with planar microcavity in normal direction at the same current density of 100 mA/cm^2 respectively. As show in Fig. 4(a), the full-width at half-maximum (FWHM) of EL spectra for devices A, B, and C at 0° are 64 nm, 104 nm, and 44 nm respectively. The wavelength dependent enhancement ratio of emission for the device A with the corrugated microcavity is calculated by dividing the spectrum at the normal direction of device A by that of the device C with the planar microcavity to show the influence of the corrugated structure on the Ag anode –Al cathode microcavity. The calculated results are shown in Fig. 4(b). Two significant peaks of enhancement ratios at short wavelength (~470 nm)and long wavelength (~650 nm) of device A can be observed, which will benefit the broad emission spectra and the higher EQE of the device A with corrugated microcavity. In traditional planar microcavity OLEDs, just like device C, performance enhancement is always wavelength dependency and angle dependency because of the confinement of the resonance mode in microcavity, and most of the generated light is trapped in the organic layer and substrate in form of waveguide modes or losted in the organic/ metal electrode interface as SPP modes [21]. So, the use of corrugated structure in the planer microcavity OLEDs, just like the device A, is expected to be a useful way to recover the trapped light [6, 7, 9]. The AFM picture of PMMA-PS film is shown in Fig. 4(c).The characteristic wavelength of the quasi-periodic structure could be obtained from the Fast Fourier Transform (FFT) pattern, as shown in the insert of Fig. 4(c). The zonal distribution features of the FFT pattern indicates the quasi-periodic nature of the corrugated structure. The power spectral density (PSD) spectrum of the PMMA-PS AFM image reveals quasi-periodic surface features of the corrugated structure, which is plotted in Fig. 4(d) as a function of the period of the grating. The PSD spectrum in Fig. 4(d) exhibits a peak value at grating period at ~600nm and a broad distribution

#225930 - $15.00 USD Received 31 Oct 2014; revised 11 Jan 2015; accepted 15 Jan 2015; published 10 Feb 2015

from grating period at 300 nm to grating period at 1200 nm. Typically, the trapped light can be extracted in air by introducing a Bragg grating with a subwavelength periodic structure, which satisfies momentum conservation in the waveguide plane [22],

$$\mathbf{k}_0 \sin\theta = \mathbf{k}_{wg} \pm n\mathbf{G} \tag{1}$$

where, $\mathbf{k}_0$ denotes the and the wave vector wave vector in free space, of the in-plane guided mode $\mathbf{k}_{wg}$ is the wave vector of the in-plane guided mode, θ is the angle of emitted light, $\mathbf{G}$ is the Bragg vector of the grating and n is an integer. In our corrugated structure, as show in the Fig. 4(c) and 4(d), the Bragg vector of the grating ($\mathbf{G}$) distributed in a broad range and over all azimuthal directions, which is expected to recover not only the waveguide mode in organic layers but also the power lost to SPP in the organic layer/metal interface.

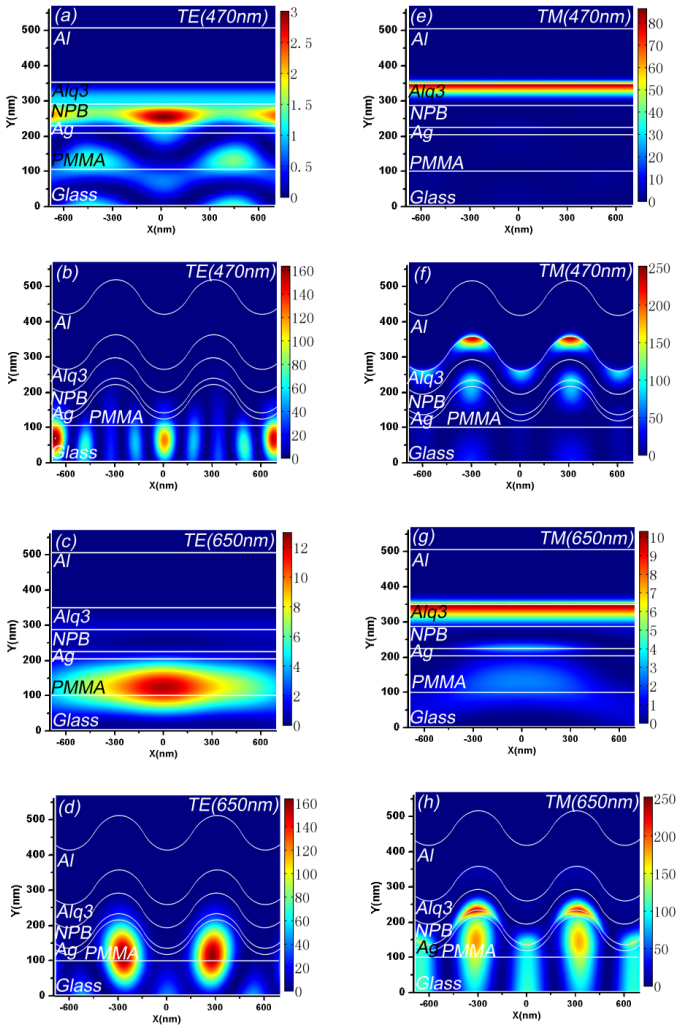

Fig. 5. (a)-(d) FEM simulated steady-state Ez field intensity distribution of TE mode for planar device at source wavelength of 470 nm (a) and 650 nm (c), for corrugated device with grating period of 600 nm at wavelength of 470 nm (b) and 650 nm (d), respectively. (e)-(h) FEM simulated steady-state Hz field intensity distribution of TM mode for planar device at wavelength of 470 nm (e) and 650 nm (g), for corrugated device with grating period of 600 nm at wavelength of 470 nm (f) and 650 nm (h), respectively.

#225930 - $15.00 USD Received 31 Oct 2014; revised 11 Jan 2015; accepted 15 Jan 2015; published 10 Feb 2015

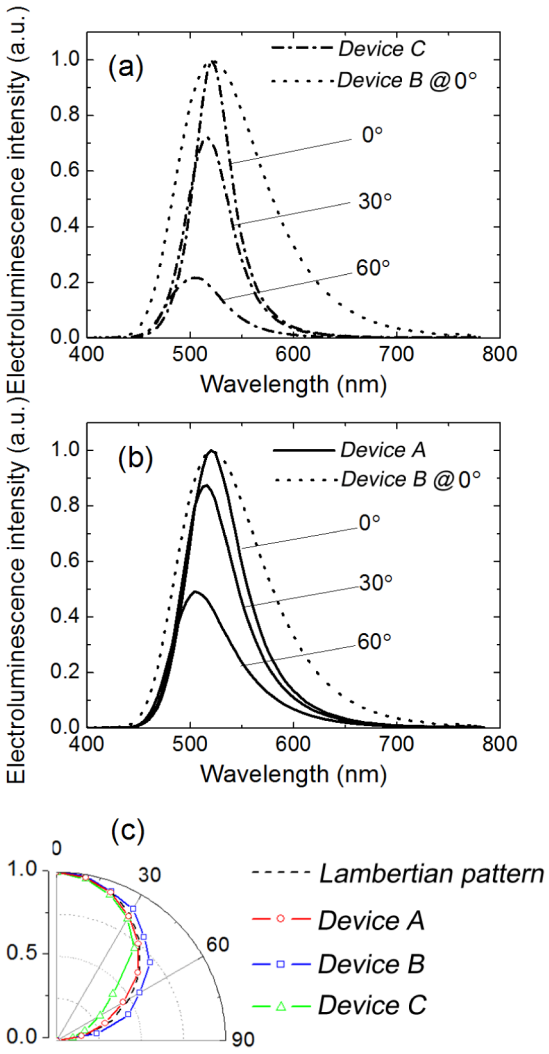

Fig. 6. Electroluminescence spectra of the device C with planar microcavity (a) and device A with corrugated microcavity (b) at viewing angles of 0°,30°and 60°respectively.The electroluminescence of device B with ITO as anode at viewing angles of 0°is also shown as an reference in (a) and (b). Emission pattern of devices A, B, and C are also exhibited (normalized to the intensity at 0°), and the Lambertian pattern is used as reference (c).

To further understand the outcoupling enhancement induced by the corrugated structure, the field intensity distribution in the corrugated device was analyzed based on Finite Element Method (FEM). Since the simulation of real quasi-periodic corrugated structure is quite complicated, a corrugated structure with a constant grating period of 600 nm, which corresponds to the peak value of grating period distribution of PMMA-PS film, was selected as a model for preliminary study. Because the SPP mode can only be excited by transverse magnetic (TM) mode, two different polarized light source with TM mode and transverse electric (TE) mode was simulated respectively. The wavelength of light source was set as 470 nm and 650 nm respectively to simulate the circumstances of the two enhancement ratio peaks of device A, just as shown in Fig. 4(b). The refractive indices of Al, Ag,NPB, Alq_3, and Glass are 1.04 + 6.57i, 0.16 + 2.26i, 1.85 + 0.02i, 1.75 + 0.02i, and 1.55 respectively. Period boundary conditions and perfectly matched layers were set along the x direction and y direction,

#225930 - $15.00 USD Received 31 Oct 2014; revised 11 Jan 2015; accepted 15 Jan 2015; published 10 Feb 2015

respectively. Device with planar structure was also simulated for comparison. The simulation results are shown in Fig. 5. Here, the steady-state Ez field intensity and the steady-state Hz field intensity are used to characterize the field intensity distribution of TE mode and TM mode respectively. The field intensity distribution of TE mode for planar device and corrugated device are shown in Fig. 5(a)-5(b). As shown in Fig. 5(a), for planar device with source wavelength of 470 nm, the light is strongly trapped as the waveguide mode in NPB layer. When the corrugated structure is added, as shown in Fig. 5(b), the waveguide mode in NPB layer is outcoupled into the glass substrate obviously. For planar device with source wavelength of 650 nm, as shown in Fig. 5(c), the light is strongly trapped in the PMMA layer. When the corrugated structure is added, as shown in Fig. 5(d), only partial waveguide mode in PMMA layer is outcoupled into the glass substrate, which indicates that, in TE mode, the outcoupling enhancement of the corrugated structure with grating period of 600 nm at source wavelength of 650 nm is not so strong as that at 470 nm. The field intensity distribution of TM mode for planar device and corrugated device are shown in Fig. 5(e)-5(h). For planar device with source wavelength of 470 nm, as shown in Fig. 5(e), the light is strongly trapped as the SPP mode at Al/Alq_3 interface. When the corrugated structure is added, as shown in Fig. 5(f), the trapped SPP mode at Al/Alq_3 interface is partially decrease. However, SPP mode that trapped in the thin Ag layer is increased. For planar device with source wavelength of 650 nm, as shown in Fig. 5(g), strong SPP mode at Al/Alq_3 interface can be observed. When the corrugated structure is added, just as shown in Fig. 5(h), light that is outcoupled to the glass substrate and the SPP mode at the thin Ag film are all increased. The SPP mode at Al/Alq_3 interface, however, almost disappears in corrugated device. Our simulation results reveal that the corrugated structure is an effective way to extract light that once trapped in planar device as waveguide mode and SPP mode. Furthermore, in the circumstances with source wavelength of 470 nm, the strong outcoupling of waveguide mode at NPB layer dominates the light outcoupling enhancement. In the circumstances with source wavelength of 650 nm, however, the outcoupling of SPP mode at Al/Alq_3 interface dominates the light outcoupling enhancement.

Figure 6 shows the angular dependence of the emission for the microcavity OLEDs with (device A) and without (device C) corrugated structure at viewing angles of 0°,30°,and 60°, compared with electroluminescence spectra of conventional ITO anode OLEDs (device B) at 0°. As shown in Fig. 6(a) and 6(b), with the increase of viewing angle, the EL peak value of device C with planar microcavity decreases quickly compared with that of the device A with corrugated microcavity. Furthermore, the FWHM of device A is broader than that of device C at the same viewing angle. Thus, device A exhibits a nearly Lambertian emission pattern, just as show in Fig. 6(c). In conventional corrugated OLEDs that fabricated on a periodic substrate, strong angular dependence are observed [13, 24]. For example, Fujita et al. found that the angular dependence property of OLEDs strongly depends on the grating period [24]. In our corrugated OLEDs, a distinct difference from one- or two-directional grating structure or photonic crystals structure is that our PS-PMMA corrugated structure having random orientation and broad periodicity. Thus, the outcoupled emission is equivalent to a stack of a series of outcoupled emission pattern from periodically corrugated OLEDs with different grating period, which makes the outcoupled emission concentrate into the normal direction. Thus, the angular dependence phenomenon is suppressed, resulting in the Lambertian emission pattern, which will benefit the light application of OLEDs.

4. Conclusions

In summary, we introduced an easy-fabricated and low cost corrugated microcavity into OLEDs and achieved large efficiency, broad spectra and Lambertian angular emission. Compared with the traditional bottom-emitting OLEDs and the planar microcavity OLEDs, our device exhibits better performance, about 57% and 41% enhancement for EQE was achieved respectively. The efficiency enhancement and the better emission features results from the Bragg diffraction effect of the quasi-periodic nature of the corrugated microcavity. Our work

#225930 - $15.00 USD Received 31 Oct 2014; revised 11 Jan 2015; accepted 15 Jan 2015; published 10 Feb 2015

provides a new approach to recover the trapped light OLEDs which will benefit the low cost fabrication OLEDs.

Acknowledgments

This work was supported by Basic Research Program of China (2013CB328705), National Natural Science Foundation of China (Program No. 61106123 and 61275034), and Natural Science Basic Research Plan in Shaanxi Province of China (Program No. 2012JQ8001).The authors also sincerely thank Mr. Dai at International Center for Dielectric Research (ICDR) in Xi'an Jiaotong University for the support of SEM measurements and Dr. Du at Key Laboratory of Photonics Technology for Information in Xi'an Jiaotong University for the suggestion in device simulation

#225930 - $15.00 USD Received 31 Oct 2014; revised 11 Jan 2015; accepted 15 Jan 2015; published 10 Feb 2015